Article

Time-resolved imaging of femtosecond laser-induced plasma expansion in a nitrogen microjet

A. G. Ciriolo[1,*,§], R. Martínez Vázquez[1,*,§], G. Crippa[1,2], M. Devetta[1], A. Frezzotti[3], D. Comelli[2], G. Valentini[2], R. Osellame[1], C. Vozzi[1], S. Stagira[1,2]

[1] National Research Council (CNR), Institute for Photonics and Nanotechnologies, Milano, Italy
[2] Politecnico di Milano, Physics Department, Milano, Italy
[3] Politecnico di Milano, Department of Aerospace Science and Technology, Milano, Italy
* these authors contributed equally to this work
* Correspondence: rebeca.martinez@polimi.it (R.M.V.), annagabriella.ciriolo@polimi.it (A.G.C.)

Featured Application: Authors are encouraged to provide a concise description of the specific application or a potential application of the work. This section is not mandatory.

Abstract: We report on the study of ultrafast laser-induced plasma expansion dynamics in a gas microjet. To this purpose, we focused femtosecond laser pulses on a nitrogen jet produced through a homemade De Laval micronozzle. The laser excitation leads to plasma excitation with a characteristic spectral line emission at 391 nm. By following the emitted signal with a detection system based on an Intensified Charge-Coupled Device (ICCD) we captured the two-dimensional spatial evolution of the photo-excited nitrogen ions with a temporal resolution on the nanosecond time scale. We fabricated the micronozzle on fused silica substrate by femtosecond laser micromachining. This technique enables high accuracy and three-dimensional capabilities, thus providing an ideal platform for developing glass-based microfluidic structures for application to plasma physics and ultrafast spectroscopy.

Keywords: De Laval nozzle; femtosecond laser micromachining; ultrafast laser sources.

1. Introduction

The development of micro-fluidic systems for controlling and manipulating the density, velocity, and composition of fluids on a micrometer scale is undergoing a great impulse over the last decade due to the advances in micro-fabrication techniques. Microstructured devices for the transport of fluids are currently employed for many scientific and technological applications ranging from micro rocket engines in aerospace technology to lab-on-chip platforms in biology and medicine [1, 2].

Miniaturization is also attracting attention in the field of atomic and molecular spectroscopy and plasma physics, with the possibility for the downsizing of large-scale workstations. Here, the delivery of a gas-phase target at controllable conditions is a fundamental requirement and is commonly accomplished by using pulsed or continuous-flow nozzles operating in a vacuum environment. The interaction of gases with the probing light sources takes place near the nozzle exit where the gas is highly confined and thermally cooled down upon supersonic expansion. Currently, the most advanced gas-delivery systems consist of electro-magnetic actuated devices producing pulsed gas jets at a repetition rate up to the kHz regime [3], eventually coupled with mechanical skimmers for particle beam velocity and trajectory selection. The repetition rate is the major limitation of pulsed valves that strongly hinder interfacing with higher repetition rate laser sources. In this framework, continuous flow systems provide a valuable solution. The most common approach consists of using gas cells and capillaries. Sophisticated continuous-flow systems based on nozzle-ended glass capillaries and enabling accurate gas velocity and temperature control were recently developed for applications to high-repetition-rate laser sources, above the MHz [4].

Dielectric-based gas-fluidic devices are particularly suitable for usage in laser-gas interaction experiments due to their high damage threshold and stability. However, to achieve proper tailoring of the gas flux, the geometry of the nozzle must be accurately engineered, down to the micrometer size, thus requiring a flexible and precise glass manufacturing technology. In this sense, Femtosecond Laser Micromachining [5] provides a powerful technique for the realization of complex microfluidic systems with high accuracy, extreme versatility, and three-dimensional capability.

Here we present a De Laval conical nozzle realized on a fused-silica slab through Femtosecond Laser Irradiation followed by Chemical Etching (FLICE). The nozzle has been designed for application to High-order Harmonic Generation (HHG) [6] and ultrafast spectroscopy. In particular, it has been thought as a component of a more complex microfluidic FLICE device aiming at achieving gas density manipulation on the micron-scale for efficient high-order harmonic generation on a chip [7]. In this work, we studied the hydrodynamic expansion of a nitrogen micro-jet in the wavefield of intense femtosecond laser pulses.

For the nozzle characterization, high-intensity femtosecond laser pulses are focused at the nozzle exit, thus interacting with the gas jet. Driven by the oscillating laser field, the gas intercepted by the laser beam may experience ionization by electron tunneling leading to the generation of electrons correlated to the parent ions [8]. In this regime, the fluorescence emission from the ionized gas at particular wavelengths in the visible/UV spectrum can be detected. Fluorescence from molecular gases provides information on the excited states involved in the strong-field processes, but can also be used for mapping the distribution of the excited molecules on a spatial domain.

In particular, we detected the radiative emission at 391 nm from $N_2^+(B^2\ \Sigma_u^+)$ to the $N_2^+(X^2\ \Sigma_g^+)$ states through an ICCD-based imaging setup. The micro-nozzle used for nitrogen injection was engineered to allow collecting the fluorescence signal in proximity to the gas jet and orthogonally to the laser propagation direction. The dynamics of the charged particle population was measured with a time step of 5 ns.

2. Materials and Methods

2.1. Glass De Laval nozzle fabrication

The fused silica micronozzles were fabricated by the FLICE technique, which allows the fabrication of 3D microfluidic devices inside a glass substrate with a maskless approach [9, 10]. A femtosecond laser beam is focused inside the glass substrate and, due to nonlinear processes that occur at the focal spot, the material is permanently modified, presenting a localized higher etching rate. By exposing the irradiated substrate to an etchant solution, it is possible to fabricate microfluidic networks with the desired geometry.

We used the second harmonic of a femtosecond laser beam (Satsuma HP, Amplitude). It provided pulses with a 270-fs duration at a 1-MHz repetition rate, and we used pulse energies ranging from 250 nJ to 380 nJ. We focused these pulses inside the fused silica substrate by a 63x microscope objective (0.75 Numerical Aperture (N.A.)) equipped with a corrective collar for spherical aberrations. The fused silica slab was mounted onto a precision 3D movement system (ANT130-035-L-ZS-PLUS and ANT95-50-XY-CMS-ULTRA from AEROTECH Inc.) that permits the movement of the sample with respect to the laser beam with an overall 275 nm accuracy. The sample was irradiated in a bottom to top direction.

The fused silica glass chip had a trapezoidal external shape with an embedded micronozzle as represented in the illustration in Figure 1. The external trapezoidal shape allowed the interaction of the gas jet with ultrafast laser pulses near the nozzle exit without damaging the device.

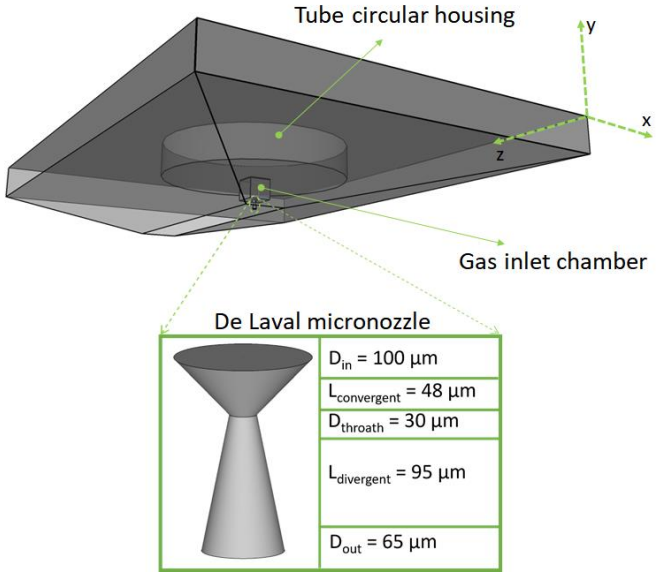

Figure 1. Illustration of the De Laval nozzle chip. The top circular housing holds the gas inlet tube (glued to it). In the blow-up image the dimensions of the de Laval nozzle are reported. The three-axis reference system we refer to within the article is reported above.

To define the gas tube reservoir and the external trapezoidal shape, the energy of the pulses used for the fabrication was fixed at 300 nJ and 380 nJ respectively, with sample translation speeds of 2 mm/s and 5mm/s. To shape the typical convergent-divergent tube geometry of a De Laval nozzle (see Figure 1 (a)), the sample was irradiated following a 3D helical trajectory with a variable radius [11]. The translation speed was 0.2 mm/s and the helix pitches (Λ) were 8 µm and 2 µm in the convergent and divergent cones respectively. The pulse energy was reduced to 250 nJ to avoid over-exposure due to the low translation speed. These irradiation conditions guaranteed a good superposition of the laser tracks.

After the irradiation, the sample was immersed in an ultrasonic bath of a 20% HF aqueous solution for 80 minutes to completely reveal the desired empty inner volumes. For the present work, we designed a De Laval micronozzle with the final geometric characteristics reported in the blow-up of Figure 1 (a). This device represents an example of the FLICE capabilities for the fabrication of micronozzles. Indeed, we can choose any arbitrary diameter (≥ 10µm), shape, and length for the different sections of the nozzle.

2.2. Experimental setup

For the study of the gas jet expansion dynamics, we used the experimental setup shown in Figure 2. The ultrashort laser pulses are provided by an ultrafast Ti:Sapphire laser system at 800 nm wavelength (Amplitude, Aurora laser system: 15 mJ, 25 fs, 1KHz). A fraction of the laser pulse energy (up to 400 µJ) was used to ionize the gas, hence triggering the plasma dynamics. We tuned the pulse energy between 150 and 400 µJ by rotating a beam splitter. The pulses were focused into a vacuum chamber by an anti-reflection coated plano-convex lens with focal length f = 300 mm. Filaments were formed in air having an elongation of ~1 cm. At the entrance, the vacuum chamber was equipped with high-optical quality fused silica windows with a thickness of 500 µm.

The nozzle was connected to the gas by a 1.5-mm inner diameter metallic tube into the glass device inlet with vacuum-compatible low-vapor-pressure epoxy glue. The metallic gas tube was interfaced with a flexible tube, thus allowing a free motion for positioning the nozzle into the experimental chamber.

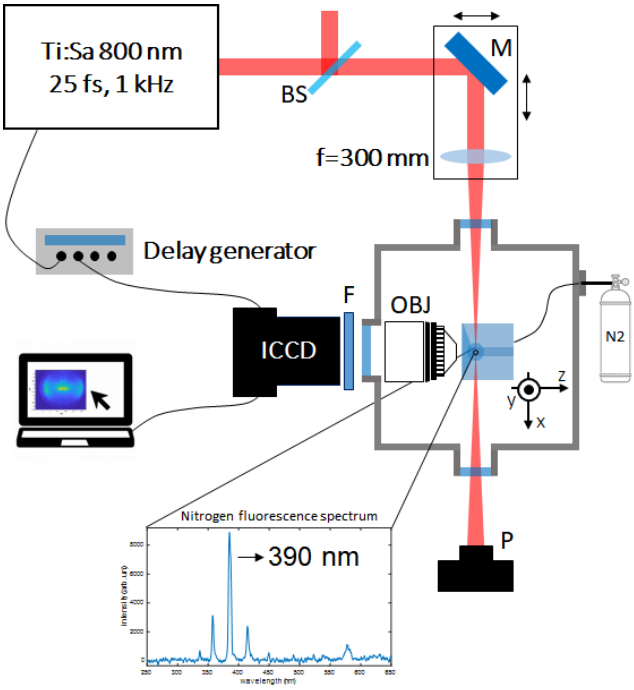

Figure 2 Experimental setup used to image the laser-excited gas dynamics. Ultrashort laser pulses were focused on the gas jet by a 300-mm focal lens. The pulse energy was modulated by a beam-splitter (BS) mounted on a rotational stage and measured by a power meter (P). The fluorescence emitted by the ionized nitrogen is collected through an ICCD interfaced with an aspheric objective (OBJ). A UV bandpass interferometric filter (F) is used to select the emission line at 391 nm. Time-resolved frames are collected by triggering the camera with a delay generator. (M) Movable mirror-lens assembly. The insert shows the fluorescence spectrum emitted by nitrogen excited with femto-second laser pulses.

The device was mounted on top of a high-precision 3-axis motorized translation system composed of three linear stages (Newport) for accurate control of the nozzle alignment to the laser filament.

The nozzle was tested in low-pressure air environment ($2 \cdot 10^{-1}$ mbar). The vacuum chamber was pumped by a dry screw pump (650 m^3/hour speed). The nozzle was loaded with a continuous backing pressure, up to 3 bars. The backing pressure can be manually tuned by a needle valve mounted upstream the gas pipeline, and accurately monitored by a capacitive pressure gauge placed after such valve.

To collect the plasma signal, we used an optical system consisting of a 30x aspheric objective lens with 0.4 N.A. (Newport, 5723-A-H), rigidly screwed on an aluminum tube mounted on a KF40 flange, and terminated with a fused silica window. For adjusting the laser beam position to the objective working distance, we put the mirror and the lens on a manual translational stage. The plasma dynamics were imaged orthogonally to the expansion direction by a fast gated camera. The camera is made by two units: a Multi Channel Plate (MCP) intensifier (C9546–03, Hamamatsu Photonics, Japan) coupled to a low noise CCD camera (Retiga R6, Q-imaging, Canada) by a lens system. The CCD camera (2688 x 2200 pixels) is operated at 2x2 binning to match the spatial resolution of the MCP (Modulation Transfer Function ≈ 1024 lines). To acquire time-resolved 2D images, we synchronized the camera acquisition with the laser pulses through a programmable time-delay generator (Stanford Research Systems, DG535). All the images were taken with gate width of 5 ns.

The spectrum emitted by nitrogen filaments in the visible down to the UV was preliminarily measured in air and a strong emission line from N_2^+ at 391 nm was detected. This spectral component was selected by using a 5-nm bandwidth interferometric filter at 391 nm (Thorlabs) placed at the entrance of the ICCD.

3. Study of the Plasma expansion dynamics

The interaction of the gas sample with the femtosecond pulses leads to the generation of a population of high-energy electrons through multiphoton ionization and electron tunnel ionization [12]. The laser-induced ionization of the gas occurs on the time scale of the pulse duration, which is significantly shorter than the characteristic gas dynamic response of the neutrals and ions undergoing expansion (≥ 10 ns). The kinetics of the plasma thus occurs under field-free conditions and involves different interaction channels among the gas species (neutrals, ions and electrons), including electron impact ionization, electron–ion recombination, and dissociative recombination [13]. In femtosecond laser filaments, the plasma decay by collisional mechanisms mainly depends on the gas density and composition, and it is commonly on the scale of tens of nanoseconds [14]. In turn, the kinetics of a plasma population governs the radiative lifetime of the emitting species. In the specific case of the 391-nm N_2^+ component, the lifetime in a filament driven by femtosecond pulses in vacuum ranges from a few nanoseconds up to tens of nanoseconds [15, 16]. In a 2D fluorescence image the information on the density distribution of the emitting species is not directly related to the intensity distribution of the fluorescence, due to the collective nature of the radiative process. Indeed, the decay of excited molecules is due to both radiative and non-radiative deactivation processes, like collisions. In this sense, the rates of radiative (k_r) and non-radiative (k_{nr}) decay mechanisms determine the emission quantum yield $\phi = k_r/(k_r + k_{nr})$, which, in turn, is strongly related to the fluorescence lifetime by $\tau = \phi/k_r$ [17]. The collisional deactivation rates mainly depends on the gas density and the mean velocity of the interacting particles, namely on the gas temperature [18, 19]. To evaluate the radiative behaviour of a plasma generated in a non-uniform gas medium, information on the electron/ion density and temperature distributions within the plasma is required. For this purpose, which is beyond the scope of our work, several techniques can be used in combination with 2D fluorescence imaging, including optical interferometry [20, 21], terahertz-based scattering [20], and pump-probe fluorescence spectroscopy [22].

To study the gas jet behavior, we traced the spatial distribution of the plasma produced by 25-femtoseconds laser pulses through the collision-mediated decay of nitrogen ions fluorescence at 391 nm. We imaged the temporal evolution of the gas excited by the 25-fs pulses, on the timescale of tens of nanoseconds, for various times after plasma onset by steps of 5 ns. Figure 3 reports the frames detected at selected delays from the laser arrival, showing the fluorescent spatial distribution of the nitrogen plasma in two different conditions, with and without the gas flux from the micronozzle.

With the scope to separate the effect of vacuum environment gas diffusion from the expansion of gas jet, we preliminarily evaluated the fluorescence emitted in a $2{\cdot}10^{-1}$ mbar vacuum environment by detecting the whole filament emission intensity in vacuum (with no gas flux from the micronozzle) as a function of time. In our experimental conditions, we measured a radiative decay characterized by an intensity peak after 10 ns from the laser arrival followed by an exponential decrease with a lifetime of 45 ns. The observation of an intensity peak delayed by 10 ns from the laser excitation suggests the early activation of non-radiative contribution and might be attributed to the effect of plasma growing under the excitation by secondary electrons. After 10 ns, the effect of secondary electrons extinguishes. In this pressure conditions, the mean free path of nitrogen molecules is estimated on the few hundreds of micrometers scale (~300 μm). Herein, collisional mechanisms play a minor role, and the characteristic fluorescence lifetime is attributed to a purely radiative decay. Figures 3(a), (b), and (c) display the radial diffusion of a portion of the plasma filament (the field of view of the imaging system ~500 μm). The laser propagation direction is orthogonal to the camera position and the pulse arrival time is con-

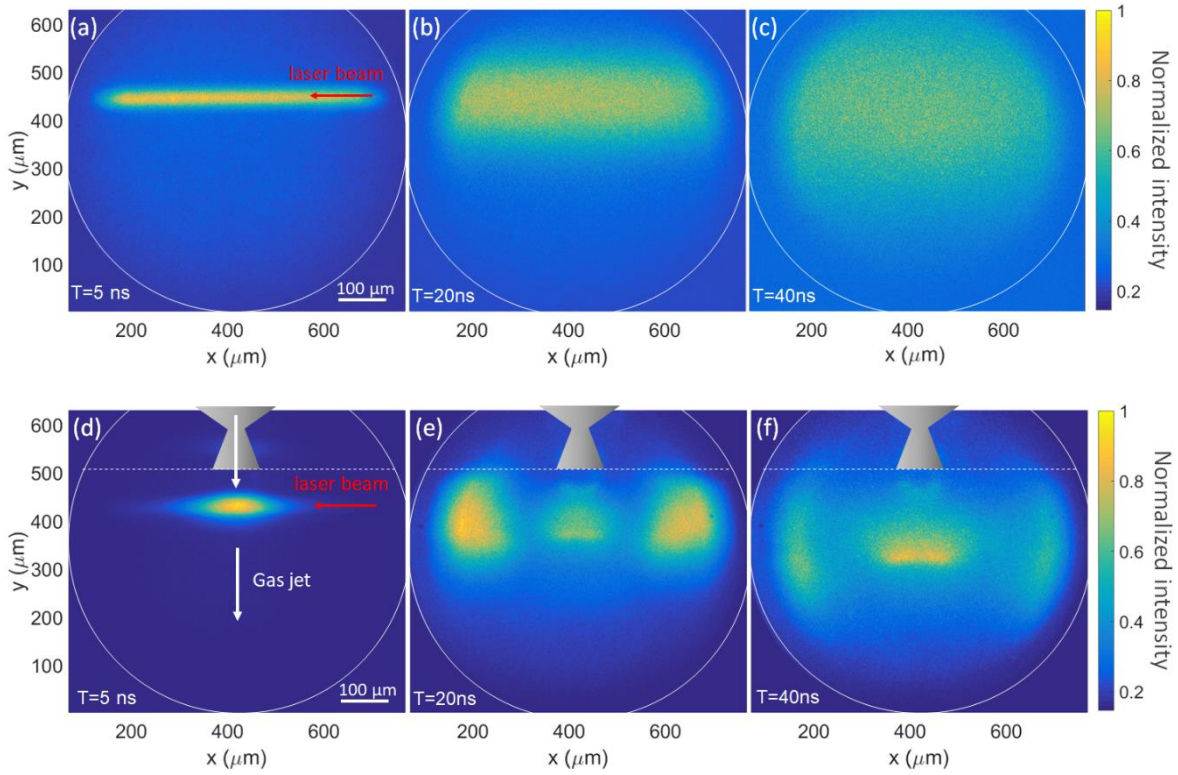

Figure 3. (a), (b) and (c) show the expansion at different time delays of a plasma filament generated by femtosecond laser pulses in vacuum ($2{\cdot}10^{-1}$ mbar). 300 μJ pulses with 25-fs duration were focused in the vacuum chamber by a 300-mm focal lens. (d), (e) and (f) show the evolution of the plasma by adding a nitrogen flux through a micronozzle loaded with a backing pressure of 3 bar. The nozzle illustration is not to scale. Each frame is normalized to the peak intensity. For each delay, the camera gain is optimized for compensating to the decay of the fluorescence emission.

ventionally indicated as T=0. After 5 ns from the pulse arrival, the fluorescence emission from the ionized molecules is strongly confined, approximately a cylinder with a diameter w=21 μm calculated as the full width at half-maximum of the Gaussian fit along the direction orthogonal to the laser propagation. Since in the first few nanoseconds after the laser arrival, the plasma kinetics can be assumed almost isochoric, the fluorescence emission at 5 ns delay provides a reasonable estimation of the initial dimension of the plasma, with w being approximately the radial extension of the gas volume ionized by the femtosecond pulses.

At longer delays (≥ 10 ns), the fluorescence signal spreads under the pressure increase inside the high-temperature conductive plasma. The radial diffusion is mainly related to the energy of the laser pulses and gas pressure [14]. Upon femtosecond laser excitation, the typical response of a low-pressure air filament is expected to produce a rapid growth of the plasma, associated with a radial increase of the nitrogen ions volume of a few microns on a time scale of a few nanoseconds. Monte Carlo simulations of nearly free molecular expansion of a hot gas column into the low-pressure cold nitrogen background, indicate that the observed time evolution of gas fluorescence is compatible with an initial gas temperature in the range [5000-10000] K. The fluorescence propagation is dominated by individual molecule motion, the average advection velocity being much smaller than the molecular thermal speed.

The expansion of the plasma generated in a gas jet was explored by using the same scheme. We positioned the glass nozzle in the laser focus at a distance d=80 μm from the laser beam (y-direction). The focal length of the focusing mirror provides a Rayleigh range much longer than the radial size of the nozzle, thus allowing for a uniform excitation of the gas jet along the beam propagation direction (x in Fig. 2), inside the interaction region. The nozzle was loaded with a nitrogen backing pressure of 3 bar. Preliminary numerical microfluidic calculations, performed with Comsol Multiphysics® [23], indicate that, in steady conditions, the axial velocity of the gas jet produced by the glass nozzle ranges between 620 m/s and 730 m/s from the nozzle outlet to a 100 μm distance, along the jet axis. Herein, the steady pressure ranges from $9 \cdot 10^2$ mbar to $1.6 \cdot 10^2$ mbar. Based on the nozzle geometry (circular throat and output with diameters respectively of 30 and 65 μm), the gas jet is expected to have a circular section in the transversal plane. From the Comsol calculations, the diameter at a beam distance d will be 85 μm, thus exceeding the radial extension of the plasma volume (w~21 μm). In this configuration, only a small portion of the gas jet is ionized by the ultrashort pulses.

Figures 3(d), (e), and (f) report time-delayed 2D maps of the nitrogen fluorescence by filamentation in the gas jet. The gas flux is directed downwards according to the image orientation.

The high nitrogen density in the focused jet produces a local increase of fluorescence intensity. At T=5 ns, the signal intensity is enhanced by almost two orders of magnitude compared to the fluorescence of the filament in vacuum (Fig. 3(a)). In particular, the intensity on the peak is higher by a factor of 76 as compared to the intensity along the plasma filament. In figure 3(d), the fluorescence emitted along the whole filament is not visible as

in figure 3(a), since the camera gain was tuned for acquiring the bright emission form the gas-jet volume.

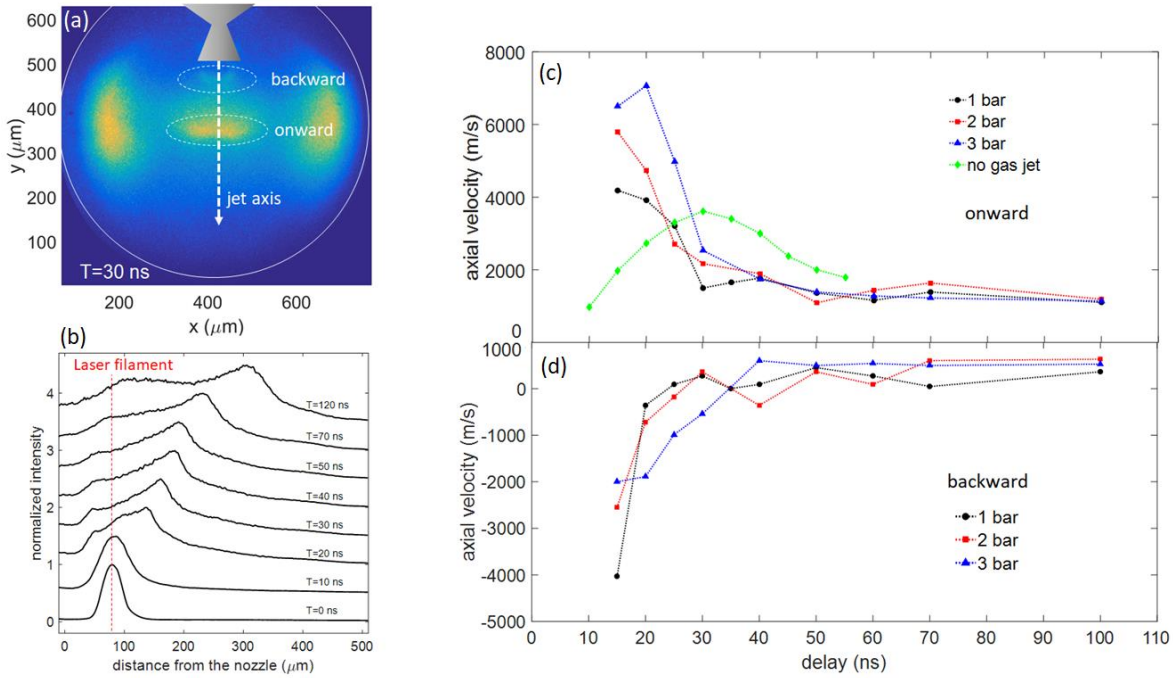

Figure 4. (a) 30-ns delayed frame showing the splitting between the onward and the backward wavefronts. (b) Fluorescence profiles along the jet axis at several delays up to 120 ns. The intensity of each curve is normalized to the peak value. (c), (d) axial velocity evolution for the onward and backward components, respectively. The propagation velocity is evaluated at three different gas pressures (1bar, 2bar, 3 bar). For sake of comparison, the green line shows the radial expansion velocity of the filaments in the absence of gas flux.

The high local density in the region corresponding to the gas jet strongly influences the spatial evolution of the plasma at later delays as suggested by the 20 ns and 40 ns delayed frames. The gas flux at the exit of the nozzle modifies the isotropic gas expansion with the appearance of a high-intensity fluorescence pattern centered on the gas jet. We expect a non-uniform fluorescence lifetime depending on the local gas density and temperature along the filament. In particular, we predict a significantly high contribution of non-radiative decay channels in the gas-jet region. Due to the non-uniform fluorescence properties, the 2D fluorescence yield of a plasma in a gas jet does not provide direct information on the gas density. However, structural information on the evolution of the lased-induced plasma can be obtained from the morphology of the fluorescence distribution. In particular, the 2D maps indicate the formation of a shock wave, associated with the generation of spatial regions with lower and higher gas density. The density wave propagates from the bulk of the excited volume isotropically, as suggested by the spherical-like shape of the low-intensity zone. In figure 3(e) and (f), two bright lobes rise at the sides of the jet and undergo a rapid lateral displacement. These two lobes correspond to low-density regions, where the fluorescence lifetime is longer and the quantum yield higher than in the jet, thus appearing brighter at longer delays.

The plasma plume confined in the central region corresponding to the gas jet evolves under the combined effect of the internal force driving expansion and external gas flux. As time increases, the plume undergoes both a spatial spreading and a splitting into two different front-waves, a brighter fluorescent feature downwards and a less intense feature closer to the nozzle (see figure 4(a)). The bright peak moves onwards along the gas-jet axis. On the other hand, the second peak is initially propagating towards the nozzle position, and undergoes a direction reversal after ~40 ns, under the effects of the nitrogen flux

from the nozzle. These two components follow different dynamics, both in terms of fluorescence decay and time-dependent propagation velocity. For sake of comparison, we report in figure 4(b) the intensity profiles along the gas jet axis as a function of the distance from the nozzle output at different time delays. At early times, the intensity distribution is composed of one peak, spatially spreading while propagating away from the nozzle. For T≥15 ns, the two counter-propagating waves rise, associated with two well-defined intensity peaks. The fluorescence undergoes a rapid decay, with a characteristic lifetime <5 ns, due to the shorter lifetime of excited nitrogen states upon the higher frequency of collisions in a dense gas jet. However, the difference between the intensity of the two wavefronts reduces in time, suggesting a faster radiative decay of the downwards component.

To quantify the plume expansion dynamics, we determined the position of the two peaks from the intensity profiles and we estimated the propagation velocity, as provided in figure 4(c) and (d). Both the two wavefronts experience a fast transitory regime during which the propagation velocity reaches values up to $7{\cdot}10^3$ m/s and $5{\cdot}10^3$ m/s for the onwards and the backward components, respectively. The velocity peak ranges between 15 ns and 20 ns from the pulsed excitation. At longer delays, the velocity converges towards a steady value. Compared to the unperturbed filament (green curve in figure 4(c)), plasma generation in a gas flux produces both faster expansion dynamics and higher propagation velocities. In this framework, we explored the dependence of both the onward and the backward shock wave components on the gas flux by changing the nitrogen backing pressure. Upon increasing the backing pressure, the onward component undergoes an increase of the expansion velocity. On the other hand, the increasing directional force opposed by the gas-jet on the propagation of the backward component produces a slower transitory response and a lower peak expansion velocity. This pressure dependence mainly affects the initial expansion dynamics by 40 ns, up to the dissipation of the thermodynamic forces driving the plasma expansion.

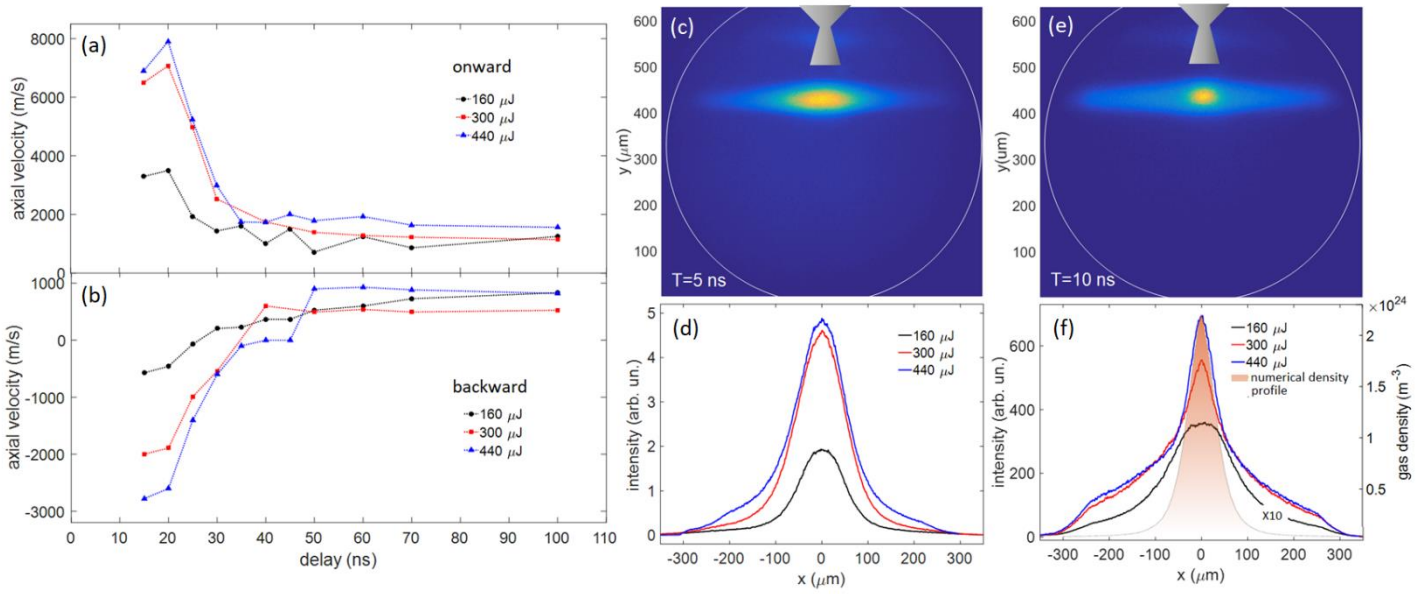

Figure 5. (a), (b) display the axial velocity evolution of the two wavefronts at different femtosecond pulse energies and fixed gas pressure (3 bar); (c) and (e) show the fluorescence generated by a 400-μJ laser pulse after 5-ns and 10-ns delays, respectively. Nozzle illustrations are on scale. (d) and (f) show the x-axis intensity profiles obtained by integrating the 2D fluorescence maps in the y-direction for different laser pulse energies at a 5-ns and 10-ns delays respectively. In panel (f), the black curve is magnified by a factor 10. After 10 ns, a narrow intensity peak rises at high energy, which reproduces the numerical gas density profile provided by the micronozzle at 3 bar.

Besides gas density, the plasma dynamics depends on the energy deposited in the ionized gas, which scales as the energy of the femtosecond laser pulses. Figures 5(a) and 5(b) provide the axial velocity of the two shock waves for different pulse energies (160 μJ,

300 μJ, 440 μJ) at fixed backing pressure of 3 bar. The onward and backward waves depend monotonically on the amount of energy transferred by the laser pulses, displaying an increase of the expansion velocity upon increasing pulse energy. We also observed a non-linear dependence of the fluorescence yield with the pulse energy. Figures 5(c) and 5(e) show the fluorescence distribution for 440-μJ pulse energy at delays 5 and 10 ns, respectively, herein a counterintuitive spatial reshaping of the fluorescence distribution can be noticed, from an elongated to a more focused bright spot. For these two delays, in figure 5(d) and (f) we report the intensity profiles along the x-direction at different pulse energies. At a 5-ns delay, the fluorescence emission consists of bell-like amplitude-scaled spatial profiles. By increasing the pulse energy from 160 to 300 μJ, the fluorescence yield scales almost proportionally, while, from 300 to 440 μJ it exhibits a saturation associated with no remarkable increase of the measured intensity. Instead, at a 10-ns delay, different pulse energies produce a considerably different fluorescence yield, which increases by more than one order of magnitude from 160 to 300 μJ, and a spatial modulation of the fluorescence distribution, which leads to a locally enhanced emission. In particular, the intensity profile along the laser propagation direction (x-axis) shows strong confinement resulting in the appearance of a narrow intensity peak at high pulse energies. Interestingly, we found a correlation between the narrow fluorescence peak rising at high pulse energy and the gas density profile as resulting from numerical microfluidics calculations in unperturbed conditions, namely unaffected by the laser field. In particular, this peak is delayed with respect to the laser pulse and progressively matches the steady-state density profile as the pulse energy increases, thus retaining information on the gas jet spatial properties preceding the plasma expansion. This behaviour suggests the activation of a different plasma decay regime depending on the energy deposited by the driving laser pulse. In a high-energy regime, Coulomb collisions among electrons start playing a crucial role due to the high density of electrons [24]. The difference in the spatial velocity distributions of heavy ions and light electrons become higher, leading to space-charge effects that affect the recombination efficiencies governing the fluorescence lifetime. In this sense, a detailed kinetic approach would be required to simulate the plasma population evolution during the expansion and to locally evaluate the radiative decay parameters as a function of the spatial properties of the plasma.

Even though the gas dynamics and the space-charge effects are in a time scale (ns) which do not affect ultrafast laser nonlinear interactions with gas in the kHz regime (Trep ~ms), it has been demonstrated that at a higher repetition rate their role is crucial. In this case, the pulse train may induce a cumulative ionization in the interaction volume leading to a steady-state plasma. The study of plasma accumulation effects is of fundamental interest for applications as XUV frequency comb generation by HHG [25]. This time-resolved 2D fluorescence imaging constitutes a powerful tool for exploring the time-resolved spatial evolution of laser-induced ionization in gas.

4. Conclusions

In this work, we applied time-resolved 2D fluorescence imaging for tracking the spatial evolution of a nitrogen plasma driven by high-energy femtosecond laser pulses. Specifically, we fabricated glass de Laval micro-nozzles by femtosecond laser micromachining followed by chemical etching. We investigated the expansion dynamics of the plasma generated in the gas microjet at different gas pressures and pulse energies by measuring the spatial distribution of the N_2^+ fluorescence at 391 nm. The measured fluorescence maps allowed us to investigate the morphology and the propagation of ions shockwaves upon continuous gas flux on a nanosecond timescale. The strong coupling between the radiative decay mechanism and the kinetics of plasma species fundamentally affect the possibility to exploit the 2D imaging scheme to fully characterize the plasma properties. On the other hand, the use of this technology coupled with conductivity and interferometric measurements as well as spectrally-resolved approaches will offer the potentials for achieving a

deeper understanding of laser-induced plasma physics, addressing interest in many research fields, including surface treatment, high-energy physics, and ultrafast optics.

Author Contributions: Conceptualization, A.F., S.S., A.G.C. and R.M.V.; validation, A.G.C., R.M.V., G.V., D.C., M.D. and G.C.; formal analysis, A.F., A.G.C., R.M.V. and G.V.; investigation, A.G.C., R.M.V., G.V., D.C, M.D. and G.C.; writing—original draft preparation, A.G.C., R.M.V. and A.F. writing—review and editing, all authors; supervision, S.S., C.V., R.O.; funding acquisition, R.O., S.S., C.V., M.D. and R.M.V. All authors have read and agreed to the current version of the manuscript."

Funding: "This project has received funding from the European Unions Horizon 2020 research and innovation program under grant agreement No 964588 (X-PIC), by the Italian Ministry of Research and Education with the projects ELI ESFRI Roadmap and PRIN aSTAR (2017RKWTMY), by the Consiglio Nazionale delle Ricerche with the Joint Laboratory ATTOBIO.

Data Availability Statement: All data needed to support the conclusions of the paper are present in the text. Raw data are available upon request.

Conflicts of Interest: "The authors declare no conflict of interest". "The funders had no role in the design of the study; in the collection, analyses, or interpretation of data; in the writing of the manuscript, or in the decision to publish the results".

References

1. A. G. Niculescu, C. Chircov, A. C. Bîrcă e A. M. and Grumezescu, Fabrication and Applications of Microfluidic Devices: A Review. *International Journal of Molecular Sciences* **2021**,, 22, n. 4, p. 2011.
2. S. Zhang, Y. Wang, P. Onck e J. and den Toonder, A concise review of microfluidic particle manipulation methods. *Microfluidics and Nanofluidics*, **2020**, 24, 4, 1-20.
3. U. Even, Pulsed supersonic beams from high pressure source: Simulation results and experimental measurements. *Advances in Chemistry*, **2014**. Author 1, A.; Author 2, B. *Book Title*, 3rd ed.; Publisher: Publisher Location, Country, 2008; pp. 154–196.
4. C. M. Heyl, S. B. Schoun, G. Porat, H. Green and J. Ye, A nozzle for high-density supersonic gas jets at elevated temperatures. *Review of Scientific Instruments* **2018**, 89, 11, 113-114.
5. K. C. Vishnubhatla, N. Bellini, R. Ramponi, G. Cerullo e R. and Osellame, Shape control of microchannels fabricated in fused silica by femtosecond laser irradiation and chemical etching. *Optics express* **2009**, 17, 10, 8685-8695.
6. A. G. Ciriolo, R. M. Vázquez, V. Tosa, A. Frezzotti, G. Crippa, M. Devetta, D. Faccialá, F. Frassetto, L. Poletto, A. Pusala, C. Vozzi, R. Osellame e S. and Stagira, High-order harmonic generation in a microfluidic glass device. *Journal of Physics: Photonics*, **2020**, 2, 2, p. 024005.
7. A. G. Ciriolo, R. M. Vázquez, A. Roversi, A. Frezzotti, C. Vozzi, R. Osellame e S. and Stagira, Femtosecond Laser-Micromachining of Glass Micro-Chip for High Order Harmonic Generation in Gases. *Micromachines* **2020,** 11 , 2, 165.
8. C. D. Lin, A. T. Le, C. Jin e H. and Wei, Attosecond and strong-field physics: principles and applications., Cambridge University Press., 2018.
9. R. R. Gattass e E. and Mazur, Femtosecond laser micromachining in transparent materials. *Nature photonics* **2008**, 2, 4, 219-225.
10. R. Osellame, H. J. Hoekstra, G. Cerullo e M. and Pollnau, Femtosecond laser microstructuring: an enabling tool for optofluidic lab-on-chips. *Laser & Photonics Reviews* **2011**, 5, 3, 442-463.
11. K. C. Vishnubhatla, N. Bellini, R. Ramponi, G. Cerullo e R. and Osellame, «Shape control of microchannels fabricated in fused silica by femtosecond laser irradiation and chemical etching. *Optics express* **2009**, 17, 10, pp. 8685-8695.
12. P. B. Corkum, Plasma perspective on strong field multiphoton ionization. *Physical review letters* **1993**, 71, 13, 1994.
13. D. Kartashov, S. Ališauskas, A. Pugžlys, M. N. Shneider e A. and Baltuška, Theory of a filament initiated nitrogen laser. *Journal of Physics B*: *Atomic, Molecular and Optical Physics* **2015**, 48, 9, p. 094016.
14. N. L. Aleksandrov, S. B. Bodrov, M. V. Tsarev, A. A. Murzanev, Y. A. Sergeev, Y. A. Malkov and a. A. N. Stepanov, Decay of femtosecond laser-induced plasma filaments in air, nitrogen, and argon for atmospheric and subatmospheric pressures. *Physical Review E* **2016**, 94, 1, p. 013204.
15. P. Wang, S. Xu, D. Li, H. Yang, H. Jiang, Q. Gong e C. and Wu, Spectroscopic study of laser-induced tunneling ionization of nitrogen molecules. *Physical Review A* **2014**, 3, 033407, 90.
16. P. Ran, G. Li, T. Liu, H. Hou e S. N. and Luo, «Collision-mediated ultrafast decay of N 2 fluorescence during fs-laser-induced filamentation. *Optics express* **2019**, 27, 14, 19177-19187.
17. J. R. Lakowicz, Principles of fluorescence spectroscopy., Springer science & business media, 2013.
18. T. Waldenmaier, J. Blümer e H. and Klages, Spectral resolved measurement of the nitrogen fluorescence emissions in air induced by electrons. *Astroparticle Physics* **2008**, 29, 3, 205-222.
19. F. Arqueros, F. Blanco e J. and Rosado, «Analysis of the fluorescence emission from atmospheric nitrogen by electron excitation, and its application to fluorescence telescopes. *New Journal of Physics* **2009**, 11, 6, 065011.

20. S. Bodrov, V. Bukin, M. Tsarev, A. Murzanev, S. Garnov, N. Aleksandrov e A. and Stepanov, Plasma filament investigation by transverse optical interferometry and terahertz scattering. *Optics express* **2011**, 19, 7, 6829-6835.
21. C. Y. Chien, B. La Fontaine, A. Desparois, Z. Jiang, T. W. Johnston, J. C. Kieffer, H. Pépin, F. Vidal e H. P. and Mercure, Single-shot chirped-pulse spectral interferometry used to measure the femtosecond ionization dynamics of air. *Optics Letters* **2000**, 25, 8, pp. 578-580.
22. A. E. Martirosyan, C. Altucci, A. Bruno, C. De Lisio, A. Porzio e S. and Solimeno, Time evolution of plasma afterglow produced by femtosecond laser pulses. *Journal of applied physics* **2004**, 96, 10, 5450-5455.
23. «COMSOL Multiphysics® v. 5.6.,» COMSOL AB, Stockholm, Sweden., [Online]. Available: www.comsol.com.
24. M. N. Shneider, A. M. Zheltikov e R. B. and Miles, Tailoring the air plasma with a double laser pulse.. *Physics of Plasmas* **2011** 18, 6, 063509.
25. G. Porat, C. M. Heyl, S. B. Schoun, C. Benko, N. Dörre, K. L. Corwin e J. and Ye, Phase-matched extreme-ultraviolet frequency-comb generation. *Nature Photonics* **2018**, 12, 7, 387-391.